Effects of Mutations in M4 of the Gastric H^+,K^+-ATPase on Inhibition Kinetics of SCH28080†

Keith B. Munson,* Nils Lambrecht, and George Sachs

Veterans' Administration Greater Los Angeles Healthcare System and Univeristy of California—Los Angeles Department of Medicine & Physiology, Los Angeles, California 90024

Received August 6, 1999; Revised Manuscript Received November 10, 1999

ABSTRACT: The effects of site-directed mutagenesis were used to explore the role of residues in M4 on the apparent K_i of a selective, K^+-competitive inhibitor of the gastric H^+,K^+ ATPase, SCH28080. A double transfection expression system is described, utilizing HEK293 cells and separate plasmids encoding the α and β subunits of the H^+,K^+-ATPase. The wild-type enzyme gave specific activity (micromoles of P_i per hour per milligram of expressed H^+,K^+-ATPase protein), apparent K_m for ammonium (a K^+ surrogate), and apparent K_i for SCH28080 equal to the H^+,K^+-ATPase purified from hog gastric mucosa. Amino acids in the M4 transmembrane segment of the α subunit were selected from, and substituted with, the nonconserved residues in M4 of the Na^+,K^+-ATPase, which is insensitive to SCH28080. Most of the mutations produced competent enzyme with similar $K_{m,app}$ values for NH_4^+ and $K_{i,app}$ for SCH28080. SCH28080 affinity was decreased 2-fold in M330V and 9-fold in both M334I and V337I without significant effect on $K_{m,app}$. Hence methionine 334 and valine 337 participate in binding but are not part of the NH_4^+ site. Methionine 330 may be at the periphery of the inhibitor site, which must have minimum dimensions of ∼16 × 8 × 5 Å and be accessible from the lumen in the E2-P conformation. Multiple sequence alignments place the membrane surface near arginine 328, suggesting that the side chains of methionine 334 and valine 337, on one side of the M4 helix, project into a binding cavity within the membrane domain.

The gastric H^+,K^+-ATPase catalyzes exchange of cytosolic protons (or hydronium ion, H_3O^+) for luminal potassium (*1*). There are two major structural classes of extracytoplasmic inhibitors of this ion-motive ATPase, the substituted pyridylmethylsulfinylbenzimidazoles (e.g., omeprazole) and the imidazo[1,2-α]pyridines (e.g., SCH28080[1] and congeners). The former attach covalently to the enzyme via disulfide bonds and are in widespread use as antiulcer drugs while the latter, reversible inhibitors are under investigation for therapeutic use. Both types of inhibitors are useful as probes for the structure and function of the enzyme since they are low molecular mass (ca 300 Da) and bind to the luminally exposed surface of the enzyme. For example, the covalent binding of the benzimidazole class of inhibitor has been used to define cysteines in the enzyme accessible from the luminal surface as part of the topographical analysis of the H^+,K^+-ATPase (*2*). These studies do not address whether the labeled cysteines are displayed above the plane of the membrane surface (in the extracytoplasmic domain) or within the membrane domain. Here we report the effects of amino acid substitutions within the membrane domain of the H^+,K^+-ATPase on the apparent affinity for the K^+ competitive inhibitor SCH28080 in order to begin to define the binding region of this reversible inhibitor.

Inhibition by SCH28080 is competitive with respect to potassium (or ammonium) activation of ATPase activity and uncompetitive with respect to ATP (*3, 4*). High-affinity binding of SCH28080 (K_d = 45 nM) is to the phosphoenzyme formed in the presence of MgATP and is similar to the $K_{i,app}$ defined kinetically (*3*). At high inhibitor concentrations (>10 μM), there is evidence for a low-affinity noncompetitive component of inhibition of dephosphorylation (*5*) indicating binding to both K^+-free and K^+-liganded phosphoenzyme resulting in mixed inhibition.

SCH28080 binds to a luminally exposed site in its charged, protonated form (*3, 4*), and a variety of protonatable amines are also K^+-competitive inhibitors of the H^+,K^+-ATPase (*6*). Their size and general lack of similarity to small cations such as K^+ and its surrogates suggest that inhibitor and ion, although mutually exclusive, interact with different side chains of the protein. The relatively high affinity of SCH28080 implies the existence of a binding site with several side chains arrayed around the inhibitor most likely contributed from different membrane segments. The dimensions, ∼16 × 8 × 5 Å (*7*), of the active conformer define the distances between acid side chains able to interact with this class of inhibitors.

The H^+,K^+-ATPase belongs to the P2 subgroup of the P-type class of phosphorylating ATPases (*8, 9*). Their defining feature is a conserved region of primary sequence around the site of phosphorylation (*10*). There is compelling

† This research was supported by SMI USVA and NIH Grants DK 41301 and DK 40615.

* To whom correspondence should be addressed: CURE, Wadsworth VA Hospital, 11301 Wilshire Blvd., Building 113, Room 324, Los Angeles, CA 90073. Fax (310) 312-9478.

[1] Abbreviations: SCH28080, 3-(cyanomethyl)-2-methyl-8-(phenylmethoxy)imidazo[1,2-α]pyridine; RMS, root mean square; sr, sarcoplasmic reticulum.

10.1021/bi991837d CCC: $19.00
Published on Web 02/24/2000

evidence for 10 membrane segments in the catalytic subunits of the P2-type enzymes, including the H^+,K^+-ATPase, Na^+,K^+-ATPases, Ca^{2+}-ATPases, *Neurospora* H^+-ATPase, and Mg^{2+}-ATPase of *Salmonella typhimurium* (*11*, *12*). Fourier transform infrared (FTIR) analysis of extensively proteolyzed sr Ca^{2+}-ATPase (as well as H^+,K^+-ATPase) membranes provided evidence that the membrane domains of these enzymes are composed largely of helices (*13*). Advances made in determining the three-dimensional structures of rat sr Ca^{+2}-ATPase (*14*) and *Neurospora* H^+-ATPase (*15*) show that density maps of the membrane domains at 8 Å resolution for these divergent P2-type enzymes are similar and appear to be fitted with 10 membrane helices (*16*). These helices are found at equivalent positions within the amino acid sequences with respect to the phosphorylation site (*17*). This site is located within a conserved cytoplasmic domain of nearly 450 amino acids between the M3M4 and M5M6 pairs of membranes segments. M3M4 is connected to the M1M2 pair of membrane segments by a second conserved cytoplasmic loop of about 120 residues. M4 has the most sequence conservation among the transmembrane segments, and the sequence connecting it to the site of phosphorylation shows high similarity in all P-type ATPases. These observations have suggested direct involvement of M4 in the mechanism of ion translocation (*18*) and resulted in selection of this segment for the mutations described here.

The various isoforms of the Na^+,K^+-ATPase have high homology (65%) to the H^+,K^+-ATPase and both require association with a β subunit (*19*). The Na^+,K^+-ATPase (α1 isoform) is insensitive to SCH28080, however, and the amino acids differing between the two enzymes in M4 were the ones initially selected for mutation. Most of the changes had no effect on $K_{i,app}$ for SCH28080 but two mutants, M334I and V337I, showed relatively large (9-fold) decreases in apparent K_i with no effect on $K_{m,app}$ for NH_4^+. This suggests mutation of these residues has little general effect on conformation but alters the binding region for SCH28080. Methionine 334 and valine 337 are located one turn from each other on the M4 helix, implying this surface forms a portion of the inhibitor site and faces a vestibule. The 8 Å density maps of the sr Ca^{2+}-ATPase and yeast H^+-ATPase each show an apparent cavity with the appropriate dimensions in the outer (luminal) half of the membrane domain (*16*), and this was suggested as a possible access path to the ion transport site (*14*). An analogous structural feature in the H^+,K^+-ATPase could provide the volume required for SCH28080 occupancy.

EXPERIMENTAL PROCEDURES

Expression Vectors for α and β Subunits of the H^+,K^+-ATPase. cDNA coding for the rabbit H^+,K^+-ATPase α subunit (*20*), GenBank accession number X64694, was inserted into the multiple cloning site of the mammalian expression vector pcDNA3.1(Zeo) (Invitrogen, Carlsbad CA) containing the eukaryotic selection marker for Zeocin resistance [plasmid pcDNA3.1(Zeo+)-H,K-α]. cDNA coding for the rabbit H^+,K^+-ATPase β subunit (*21*), GenBank accession number M35544, was inserted into the multiple cloning site of the mammalian expression vector pcDNA3-(G418) (Invitrogen, Carlsbad CA) containing the eukaryotic selection marker for G418 resistance [plasmid pcDNA3.1-(G418)-H,K-β].

Production of α Subunit Mutations Y324C/R328E, M330V, V331I, F333L, M334I, A335G, V337I, and Y340N. Mutations were generated by using the two-step PCR mutagenesis protocol (*22*). Briefly, sense and antisense primers enclosing the mutation sites were used in separate PCR reactions with respective sense and antisense "outside" primers T7 (in the T7 promoter site 72 bases to the 5′ side of a unique *Eco*RI site, 20 bases before the α start codon) and "85A" (beginning at position 1723 in the α gene sequence, 681 bases to the 3′ side of a unique *Nhe*I site). A second PCR reaction utilized the outside primers with the gel-purified products of the first PCR reaction acting as overlapping templates. The final PCR products were then digested with *Eco*RI and *Nhe*I and used to replace the equivalent section of the α sequence in pcDNA3.1(Zeo)-H,K-α. The amino acid substitutions (codons underlined) and sense primers were as follows:

R328E	ACACCTTCCTGGAGGCCATGGT CTTCTT
M330V	TCCTGCGGGCCGTGGTCTTCTTCAT
V331I	CTGCGGGCGATGATCTTCTTCATGGC
F333L	CATGGTCTTCCTCATGGCGATTGT GGTAGC
M334I	GGTCTTCTTCATAGCCATTGTGG TAGC
A335G	GGTCTTCTTCATGGGCATTGTGG TAGC
V3371	GCCATTATTGTAGCCTATGTG CCCGAG
Y340N	ATTGTGGTAGCCAACGTGCCCGAGG

Plasmids were sequenced over the range of the insert to verify each mutation. Sequencing revealed plasmid "R328E" was a double mutant, Y324C/R328E, and this was characterized in lieu of R328E.

Transfection of HEK293 Cells and Selection of Stable Cell Lines. Human embryonic kidney cells (HEK293-ATCC CRL 1573) at 75% confluence in 100 mm culture plates were transfected by using the calcium phosphate method (calcium phosphate transfection kit, Invitrogen, Carlsbad CA) and 20 μg of pcDNA3(G418)-H,K-β plasmid. After 72 h, the transfected cells were submitted to selection in the presence of 0.75 mg of G418/mL of medium for 7 days. The resulting colonies were examined on Western blots with a monoclonal antibody against the β subunit. A clone with high β subunit expression was isolated, saved, and grown in the presence of 0.25 mg of G418/mL of medium. This cell line was used for a second calcium phosphate transfection with either wild-type or mutant pcDNA3.1(Zeo)-H,K-α plasmid. The transfected cells were maintained at 0.25 mg of G418/mL of medium for 72 h and then selected in the presence of the same concentration of G418 and 0.4 mg of Zeocin (Invitrogen, Carlsbad CA) per mL of medium. After 7 days individual colonies were expanded under maintenance concentrations of G418 and Zeocin (0.25 mg/mL and 0.1 mg/mL, respectively) and examined on Western blots for stable α and β subunit expression. Double selection with G418 and Zeocin resulted in colonies with high frequency (88%, n = 110, 22 different mutants) of full-length α subunit expression. The amount of α subunit per 10^5 cells (assayed by Western

blot) varied approximately 10-fold. Two clones with the highest ratio of α subunit expression to total protein were saved and expanded for each mutant. In addition, the remaining colonies on the plate were expanded together to give a mixed colony preparation.

Preparation of Crude Membranes. Cell layers from stable or mixed cell lines were grown to confluence, rinsed with phosphate-buffered saline (PBS), and then treated for 2 min with distilled H_2O at 4 °C. The H_2O was poured off and the osmotically broken cells were resuspended in Na^+-free buffer A [PIPES (10 mM)/EGTA (2 mM)/EDTA (2 mM), pH 7.0]. The cell suspension was homogenized with a tight Dounce homogenizer (Wheaton). The homogenate was submitted directly to centrifugation at 75000*g* on 40% sucrose (w/v) in buffer A for 1.5 h at 4 °C. The interface membranes were diluted to a total volume of 15 mL with buffer A and collected by centrifugation at 65000*g* for 45 min at 4 °C. The pellet was resuspended in buffer A and homogenized in a 2 mL Teflon homogenizer (final protein concentration ~5 mg/mL). The protein concentration was measured by the Lowry method with bovine serum albumin as a standard (*23*). The membranes were flash-frozen in liquid nitrogen and stored at −80 °C.

SDS−PAGE and Western Blot Analysis. Gel samples consisting of 2−20 μg of wild-type or mutant membrane protein were separated on SDS−6% polyacrylamide gels with a 4% stacker gel using the Laemmli sample and buffer system (*24*). Purified G1 fraction (*25*) gastric vesicles (40−120 ng of protein) were used as a standard to quantitate the amount of H^+,K^+-ATPase protein expressed. Prestained, high molecular weight standards (Bio-Rad Laboratories, Hercules, CA) were used to monitor the progress of electrophoresis. After SDS−PAGE, proteins were transferred to nitrocellulose membranes (BioPlot-NC, Costar, Cambridge, MA). Membranes were washed twice with Tris-buffered saline [TBS; 10 mM Tris, 150 mM NaCl, and 0.05% Tween (v/v)] and incubated in TBS containing 5% (w/v) nonfat milk (Carnation). After 30 min, the membranes were incubated in the primary antibody solution made with monoclonal antibody HK 12.18 diluted 1:2000 in TBS (recognizing amino acids 666−689 of the α subunit). After 1 h, membranes were washed twice with TBS and incubated with the secondary antibody solution (anti-mouse IgG conjugated to alkaline phosphatase, Promega, Madison, WI, diluted 1:500 in TBS). After 1 h, membranes were washed twice and incubated for 15 min in TBS. After a final wash, the membranes were incubated for 15 min in AP buffer (100 mM Tris, 100 mM NaCl, and 5 mM $MgCl_2$, pH 9.5) containing 0.3% nitro blue tetrazolium solution (v/v) and 0.15% 5-bromo-4-chloro-3-indolyl-l-phosphate solution (v/v) according to the manufacturer's instructions (Promega, Madison, WI).

Quantification of Expressed H^+,K^+-ATPase. Stained Western blots were scanned on a flatbed scanner (Hewlett Packard ScanJet 3C) and the optical density of the α subunit bands was quantified by using the software program Image, version 1.31, by W. Rasband, Research Services Branch, NIH. A curve of staining density versus total protein in a standard G1 preparation of purified hog gastric H^+,K^+-ATPase was generated and the α subunit staining densities of each mutant on the same blot were used to determine the equivalent amount of H^+,K^+-ATPase protein expressed in a known amount of their total membrane protein. The fraction of H^+,K^+-ATPase protein measured in all clones examined ranged between 1.0% and 5.0% of the total membrane protein. Integration of the 280 nm absorption peaks after gel filtration shows more than 85% of the G1 protein is composed of the α and β subunits. Hence the activity in each mutant could be expressed as a specific activity (micromoles of P_i per hour per milligram of expressed H^+,K^+-ATPase protein) based on the nearly pure G1 standard.

NH_4^+-Stimulated ATPase Activity. Wild-type and mutant membranes were analyzed for their ion-stimulated ATPase activity by the method of Yoda and Hokin (*26*). Assays measured liberation of radioactive phosphate from [γ-^{32}P]-ATP at 37 °C in Na^+-free medium with 10−30 μg of membrane protein containing between 0.1 and 0.3 μg of expressed H^+,K^+-ATPase. The reaction solutions contained final concentrations of 0.4 mM [γ-^{32}P]ATP, 40 mM Tris-HCl, and 2 mM $MgCl_2$, pH 7.4, in a volume of 150 μL. The ATP concentration was well above the high-affinity K_m (50 μM) and was never more than 50% consumed. Various inhibitors were added to suppress possible background ATPases, including 1 mM EGTA (Ca^{2+}-ATPases), 500 μM ouabain (Na^+,K^+-ATPase), 1 μM oligomycin (mitochondrial ATPase), 10 nM bafilomycin (V-type ATPases), and 100 nM thapsigargin (SERCA ATPases). Triplicate ATPase assays were performed without added ion and with various NH_4^+ concentrations in the presence or absence of several concentrations of SCH28080, the specific, K^+-competitive inhibitor of the H^+,K^+-ATPase. NH_4^+ was used in lieu of K^+ to prevent acidification of ion-tight vesicular space and to avoid use of an ionophore (*27*). All reactions were initiated by adding 2.4 mM ([γ-^{32}P]-ATP (specific radioactivity of 10^4 cpm/nmol). [γ-^{32}P]ATP (3000 Ci/mmol) was obtained from Amersham Pharmacia Biotech. The reactions were terminated after 1 hr at 37 °C by adding an equal volume of 4.5% ammonium molybdate in 14% perchloric acid, 4 °C. Quenched reaction mixtures at 4 °C were extracted with 300 μL butyl acetate and ^{32}Pi measured by scintillation counting.

The membrane concentrations of wild-type and mutant enzymes were usually adjusted so that the ATPase activation ranged from $\sim(2.0 \times 10^4) \pm 10^3$ cpm above background [$10^5 \pm (5.0 \times 10^3)$ cpm] in the lowest ammonium concentration (1.0 mM) to $\sim 10^5 \pm (5.0 \times 10^3)$ cpm above background for the highest ammonium concentration (28 mM). Over a much lower range of counts it was possible to collect kinetic data for mutants with specific activities as low as ~2% of wild type in clones selected for high expression.

Rates in micromoles of ATP hydrolyzed per hour (or micromoles of P_i released per hour) were normalized to the amount of H^+,K^+-ATPase (G1 fraction) protein, yielding equivalent α subunit staining to the mutant assayed by Western blots. Activity plots therefore show specific activity (micromoles of P_i per hour per milligram of H^+,K^+-ATPase protein).

Kinetic Analysis. For purified G1, inverse plots intersect on the ordinate axis with increasing SCH28080. Binding of activating ion (either ammonia or potassium) and inhibitor to the enzyme is therefore mutually exclusive. Potassium (or ammonium) activates the fast phase of dephosphorylation, and this is the step inhibited by SCH28080 in G1 (*5*). A simplified mechanism analogous to the classical Michaelis−Menten treatment for simple linear competitive inhibition

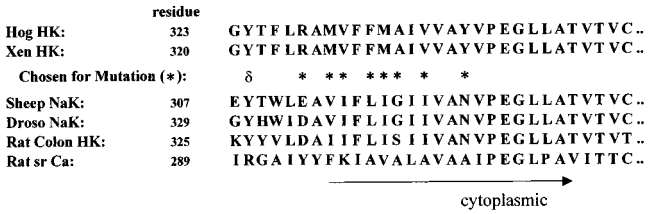

FIGURE 1: Multiple sequence alignment in transmembrane region M4. Upper aligned sequences (hog and *Xenopus* H^+,K^+-ATPases) show high-affinity inhibition by the K^+-competitive inhibitor, SCH28080, whereas those below show insignificant inhibition. Residues selected for mutation (*) to their sheep Na^+,K^+-ATPase counterparts are conserved in the SCH28080-sensitive enzymes. Abbreviations show species (and tissue type or cellular location) and then ion(s) transported: hog HK (*39*), sheep NaK (*40*), rat colon HK (*41*), Droso NaK (*42*), Xen HK (*43*), and rat (sr) (*44*). Tyrosine 324 (*δ*) was mutated to cysteine as part of a double mutant Y324C/R328E.

was used to interpret the majority of the results and is used again here (*5*).

Data were first fitted to the Michaelis−Menten equation via nonlinear regression and then replotted in inverse form for visualization of the tendency to approach a constant $1/V_{max}$. Plots generated in the absence of inhibitor yield the V_{max} (the maximum specific activity as plotted) and the apparent K_m ($K_{m,app}$) for ammonium. Replots of the slopes versus inhibitor concentration give the apparent $-K_i$ ($K_{i,app}$) as the intercept at the abscissa.

In addition to purely competitive inhibition, there is also evidence for much lower affinity SCH28080 binding simultaneously with potassium (*5*). Such a noncompetitive component of binding when combined with competitive inhibition gives rise to mixed inhibition. When kinetics are not purely competitive, plots of inverse velocity versus inverse ion concentration intersect to the left of the vertical axis and below $1/V_{max}$. $K_{i,app}$ is obtained graphically via replots of the inverse slopes versus inhibitor concentration in the same way as for competitive inhibition, whereas replots of $1/V_{max,app}$ versus inhibitor concentration give $-\alpha K_i$ as the horizontal intercept. Here, values of α above ∼15 indicate that the apparent affinity of noncompetitive binding is ∼15-fold less than that of competitive binding, and these fall within the scatter of the best data obtained. Mutants above this threshold were considered as competitive. Only two mutants seemed to show mixed inhibition.

Selection of Mutants. Mutants created in M4 were based on sequence alignments of SCH28080-sensitive and insensitive P2-type ATPases (Figure 1). These included two divergent species with high apparent affinity for SCH28080, *Xenopus* and porcine H^+,K^+-ATPase, and three others representing those with low affinity, sheep and *Drosophila* Na^+,K^+-ATPase, and rat colonic H^+,K^+-ATPase, a probable Na^+,K^+ antiporter (*28*). Residues in the SCH28080-sensitive H^+,K^+-ATPase not conserved in the Na^+,K^+-ATPase were chosen for mutation (indicated with asterisks in Figure 1 and listed in Table 1). In each case, mutations were to the corresponding sheep Na^+,K^+-ATPase residue.

RESULTS

Western Blot Quantitation. Membrane preparations for each mutant were assayed for total protein and submitted to Western blot analysis with an antibody highly specific for the gastric H^+,K^+-ATPase α subunit. Positive clones gave single bands, which were quantitated by densitometry. A standard curve of α subunit staining density versus protein in purified hog gastric G1 vesicles was generated and used to determine the amount of H^+,K^+-ATPase protein (α and *β* subunits) expressed in a given amount of total mutant membrane protein. The specific activities of each mutant (micromoles of P_i per hour per milligram of expressed H^+,K^+-ATPase protein) could then be compared directly to that of the G1 preparation where more than 85% of the total protein is α and *β* subunits. A representative blot showing this method (Figure 2) compares different amounts of H^+,K^+-ATPase purified from hog gastric mucosa (G1 fraction, *25*) to membranes from a clone selected for high expression of the Y340N mutant (clone 4, where 5.3% of the membrane protein is H^+,K^+-ATPase) and the corresponding mixed-colony membranes (1.6% H^+,K^+-ATPase). Typically, mixed-colony membranes had lower expression and this example

Table 1: Specific Activity, Apparent K_m for Ammonium ($K_{m,app}$), and Apparent K_i for SCH28080 ($K_{i,app}$) in Tissue-Purified, Wild-Type, and Mutant H^+,K^+-ATPases[a]

enzyme	data sets (*n*)	$K_{m,app}$ (mM)	specific activity [%]	$K_{i,app}$ (nM)
gastric HK-ATPase[b]	3	2.7 ± 0.1	72 ± 1 [100]	107 ± 18
wild-type (clones 3 and 28)	5	2.3 ± 0.5	66 ± 13 [92]	101 ± 35
Y324C/R328E (mixed)[c]	3	0.7 ± 0.3	24 ± 3 [33]	165 ± 30
M330V (clone 6)	3	3.3 ± 0.6	41 ± 8 [57]	229 ± 26
V331I (mixed)	2	2.5 ± 0.8	41 ± 11 [57]	80 ± 22
F333L (clone 3)	2	3.6 ± 0.3	58 ± 6 [81]	160 ± 42
M334I (clone 7)	1	3.2 ± 1.4	29 ± 4 [40]	843 ± 252
M334I (clone 15)	1	4.6 ± 1.3	30 ± 3 [42]	962 ± 111
A335G (clone 4)	3	6.4 ± 1.4	27 ± 6 [38]	51 ± 40
V337I (mixed)	2	2.6 ± 0.4	47 ± 2 [65]	893 ± 94
Y340N (clone 4)	3	1.6 ± 1.0	2 ± 1 [3]	140 ± 80

[a] Data were derived from initial velocity experiments as described in the text and Figure 3. Specific activity is given in micromoles of P_i per milligram of H,K-ATPase protein per hour. Errors were calculated from nonlinear regression fits to the Michaelis−Menten equation except for wild type, where the values are the mean and standard deviation of five experiments. Activities ranged from a high of 1.8 (wild type) to 0.1 (Y340N) in units of micromoles of P_i per hour for total membrane protein. [b] H,K-ATPase G1 fraction from hog gastric mucosa (*25*). [c] Mixed indicates a mixture of clones selected for mutant H,K-ATPase expression.

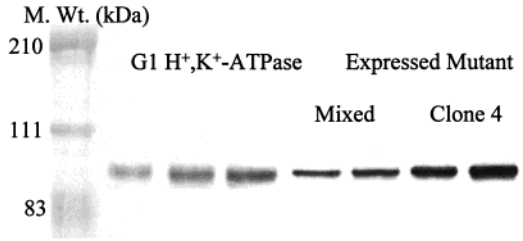

FIGURE 2: Representative Western blot comparing purified gastric H^+,K^+-ATPase [G1 fraction, (*25*)] to mutant membranes. Membranes were isolated either from a mixture of expression clones or from an individual clone (clone 4) selected for high expression. Total protein loaded onto gels: 40, 80, and 120 ng of G1, 4.8 and 9.6 μg of mixed clonal membranes, or 4.4 and 8.8 μg of clone 4 membranes. Bands were quantitated by densitometry and a standard curve of α subunit staining intensity versus nanograms of G1 was used to determine the amount of H^+,K^+-ATPase expressed. The calculated amounts were 0.017 and 0.053 μg of H^+,K^+-ATPase expressed/μg of membrane protein for Y340N mixed colony and clone 4 preparations, respectively.

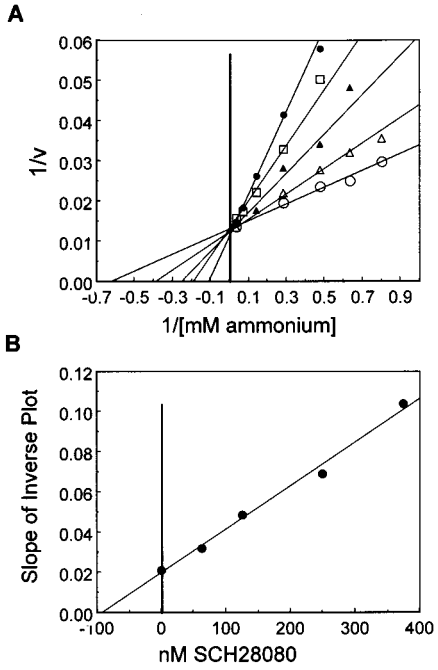

FIGURE 3: Kinetics of expressed wild-type H^+,K^+-ATPase (clone 28) in the presence of various concentrations of ammonium and 0 (○), 60 (△), 120 (▲), 240 (□), or 360 (●) nM SCH28080. (A) Rates were corrected for the amount of H^+,K^+-ATPase protein measured on Western blots. Plots therefore show inverse specific activities [(micromoles of P_i per milligram of HK-ATPase protein per hour)$^{-1}$] versus inverse ammonium concentration [(millimolar)$^{-1}$]. All lines were drawn by using V_{max} and K_m obtained from nonlinear regression fit of the data to the Michaelis−Menten equation (Enzfitter for MS-DOS, Robin J. Leatherbarrow, Elsevier-Biosoft, 1987). (B) Replots of the inverse line slopes versus inhibitor concentration are linear and intersect the horizontal axis at $-K_i$ for either linear competitive or linear mixed inhibition.

illustrates a case where expansion of a clone giving high expression was required to obtain a measurable level of activity above background.

Ammonium-Stimulated ATPase in Wild-Type Membranes. Ammonium-stimulated initial velocity assays were performed on wild-type or mutant membranes over ranges of ion and inhibitor concentrations appropriate for their apparent K_m and K_i with higher concentrations of inhibitor required for the less sensitive mutants. A representative data set is shown in Figure 3 for wild-type H^+,K^+-ATPase (clone 28). The inverse plots (Figure 3A) intersect on the ordinate axis, consistent with competitive inhibition, and the slope replots (Figure 3B) are linear. In this experiment the kinetic constants were $K_{m,app} = 1.6 \pm 0.1$ mM NH_4^+, $V_{max} = 77 \pm 2$ μmol of P_i h^{-1} (mg of H^+,K^+-ATPase protein)$^{-1}$, and $K_{i,app} = 90 + 11$ nM SCH28080. Values from five experiments using two different wild-type clones were $K_{m,app} = 2.3 \pm 0.5$ mM NH_4^+, $V_{max} = 66 + 13$ μmol of P_i h^{-1} (mg of H^+,K^+-ATPase protein)$^{-1}$, and $K_{i,app} = 101 \pm 35$ nM SCH28080 (Table 1). Standard deviations in the kinetic constants were 33% or less, and changes greater than 1.5-fold in the various mutants were considered significant.

Kinetic analysis of G1 gave $K_{m,app} = 2.7 \pm 0.1$ mM, $V_{max} = 72 \pm 1$ μmol (mg of protein)$^{-1}$ h^{-1}, and $K_{i,app} = 107 \pm 18$ nM, with all lines intersecting on the vertical axis. These results show that rabbit H^+,K^+-ATPase expressed in HEK293 cells as described here is functionally equivalent to enzyme purified from the hog gastric mucosa with the same apparent maximum turnover rate (micromoles of ATP hydrolyzed per hour per mole of α/β oligomer) and the same apparent ion and inhibitor sites ($K_{m,app}$ and $K_{i,app}$).

Effects of Mutations on Specific Activity. Mutants M330V, V331I, F333L, and V337I showed nearly normal specific activity, while Y324C/R328E, M334I, and A335G had slightly lower specific activity (about a third of wild type) as shown in Table 1. Mutant Y340N substitutes a potential ion-binding side chain one turn of the helix from a glutamate thought to be involved in ion binding. This mutant was nearly inactive (~3% of wild type) and the possibility of a Na^+ requirement for activity was tested. The SCH28080-sensitive ATPase activity was the same, however, in the presence of ouabain and either 10 mM KCl or 10 mM KCl plus 20 mM NaCl, showing no conversion to Na^+,K^+ ATPase specificity (data not shown).

Effects of Mutations on Ion and SCH28080 Affinity. Ion activation was not significantly affected in the mutants with the exception of Y324C/R328E and A335G, whose apparent ammonium affinities were 3-fold higher and 3-fold lower, respectively, than those of wild type. Parallel changes in $K_{i,app}$ were not observed for these mutants. Y324C/R328E had essentially wild-type affinity for SCH28080 and A335G, a 2-fold higher apparent affinity ($K_{i,app} = 51$ nM). No significant change in $K_{i,app}$ was found for mutants V331I or F333L. In contrast, SCH28080 affinity was decreased 2-fold in M330V and 9-fold in V337I and M334I. Separate clones (7 and 15, Table 1) were tested in the case of M334I and gave similar results. Inhibition was competitive in all mutants with the exception of F333L and V337I, whose mixed inhibition was characterized by α values of 15 and 7, respectively (i.e., the noncompetitive components of inhibition were 15- and 7-fold lower in apparent affinity, respectively, than the competitive component, see above). Hence, inhibition even in these two mutants was still predominately competitive. Changes in $K_{m,app}$ or $K_{i,app}$ with the Y340N mutation were insignificant compared to wild type, suggesting lack of involvement of Y340 in ion or inhibitor binding.

DISCUSSION

The expression and ATPase assay protocols applied to the expressed enzyme reflect the native state of the gastric H^+,K^+-ATPase as shown by the equivalence of the $K_{m,app}$ (ammonium), $K_{i,app}$ (SCH28080), and V_{max} found in the expressed wild-type ATPase to the tissue-derived G1 enzyme (Table 1). Only one of the mutants tested was severely inactivated (Y340N), and here, no large effects were found on apparent ion affinity ($K_{m,app}$). Three-fold changes in $K_{m,app}$ were found for Y324C/R328E and A335G, with increased and decreased apparent affinities, respectively. A335G also showed an apparent 2-fold increase in SCH28080 affinity. An increase in backbone flexibility associated with the removal of the side-chain methyl may account for the effects in A335G. The absence of large changes in specific activity and $K_{m,app}$ in the remaining mutants suggested the protein structure was not significantly altered from native enzyme. In these mutants, effects on $K_{i,app}$ can then be interpreted most readily as directly affecting SCH28080 interaction with the enzyme and not on overall conformation.

Large decreases (9-fold) in apparent SCH28080 affinity were found for M334I and V337I and a smaller (2-fold)

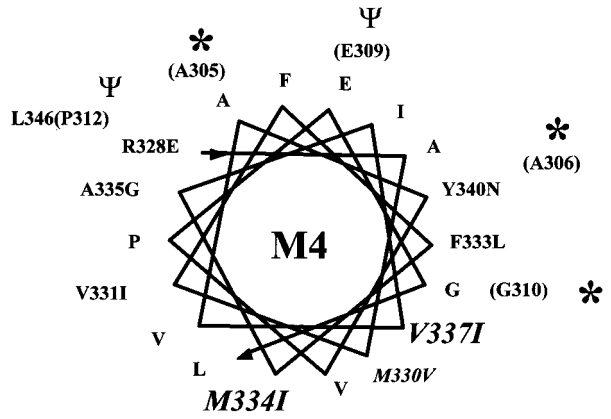

FIGURE 4: Helical wheel for the M4 region of the H^+,K^+-ATPase α subunit starting at arginine328 (arrow). Numbered residues indicate the mutations investigated. Mutants with either 2-fold (M330V) or 9-fold (M334I and V337I) lower apparent affinity for SCH28080 appear on one side on the helix (italicized). Residues (parentheses) important for either the E2-P to E2 (*) or E1-P to E2-P (Ψ) conformational changes in the sr Ca^{+2}-ATPase (*29*) are shown in their corresponding M4 positions.

decrease was seen for M330V. A helical wheel beginning with arginine 328 (Figure 4) shows the orientation of these residues in M4. In the sr Ca^{+2}-ATPase the M4 helix is presumed to include isoleucine 298 after lysine 297 (*29*). Sequence alignments match isoleucine 298 with phenylalanine 332 of the HK-ATPase, placing methionine 334 and valine 337 within the helix as shown in Figure 4. If arginine 328 is close to the plane of the membrane surface, methionine 334 and valine 337 would be at least one helix turn within the membrane domain of the protein rather than in the extracytoplasmic domain. Interaction of the imidazo[1,2-α]-pyridines has been shown to be only from the lumen (*30*) and the inhibitor must therefore gain entry to its site from the extracytoplasmic side of the membrane. Methionine 334 and valine 337 apparently lie within an opening or path at least large enough to accommodate SCH28080 and allow its entry from the extracytoplasmic milieu.

Earlier characterization of a radioactive, photoaffinity analogue of SCH28080, 8-[(4-azidophenyl)methoxy]-1-tritiomethyl-2,3-dimethylimidazo[1,2α]pyridinium iodide, localized K^+-sensitive, light-dependent labeling to a 15 kDa peptide containing the M1 and M2 transmembrane segments (*30*). It was proposed that part of the binding site was formed by the extracytoplasmic loop between M1 and M2. Various mutations in the second half of M1 and replacement of the loop between M1 and M2, however, showed no effect on inhibition by SCH28080 (*31*), indicating important binding-site residues are not in this extracytoplasmic loop. On the other hand, binding within the membrane domain implies an opening exists between helices or helix pairs to enable several side chains to form a binding pocket. Since the photoreactive azido group is attached at the *para* position of the phenyl moiety of the photoaffinity inhibitor, the labeling site is presumably at one end of the binding pocket, perhaps deeper into the membrane domain than anticipated previously. The dimensions of SCH28080 (~16 × 8 × 5 Å) are large compared to most of the interhelix distances found in the membrane domains of the sr Ca^{+2}-ATPase and yeast H^+-ATPase. A luminally exposed crevice or vestibule lined by several transmembrane helices is seen, however, in the 8 Å density maps of both sr Ca^{+2}-ATPase and yeast H^+-ATPase (*16*). This was proposed as a possible point of ion entry (*14*). A similar feature in the H^+,K^+-ATPase may provide the SCH28080 binding site, which presumably would include contributions from other side chains besides methionine 334 and valine 337. Either M1 or M2 at the periphery of the vestibule might react with the photolabile end of the photoaffinity reagent and these residue(s) remain to be identified.

A more recent sr Ca^{2+}-ATPase density map at 3.7 Å resolution (S. Toyoshima, personal communication) places the M4 helix adjacent to the membrane crevice seen earlier at 8 Å (*16*). Sequence conservation leading through M4 to the site of substrate phosphorylation suggests direct participation of this region in the mechanism and makes defining the orientation of the M4 helix in E1 and E2 conformations of clear significance. Predicting the orientation of the M4 helix is difficult because of its sequence conservation, not allowing identification of the bilayer facing residues as those that are not greatly conserved (*32*). The results presented here suggest placing the methionine 334 and valine 337 side chains toward the vestibule in E2. In contrast, the adjacent and opposite sides of M4 appear to be involved in protein/protein contact. Toward the cytosolic side and on the surface next to and across from V337 (see Figure 4), the corresponding positions in the sr Ca^{2+}-ATPase have been shown to be involved in conformational transitions, either E1-P to E2-P or E2-P to E2. Hence complete loss of Ca^{2+} uptake was given by different substitutions at positions 305, 306, 309, 310, and 312 in the sequence $A_{(305)}$-A-I-P-E-G-L-P, with impairment of the E2-P to E2 conformational transition in mutants at positions 305, 306, and 310 and impaired E1-P to E2-P transitions for mutants at 309 and 312. These results suggest protein−protein contacts on this patch of the helix surface (Figure 4) and are supported by the loss of activity in the Y340N mutant where the Na^+,K^+-ATPase residue, asparagine, is virtually incapable of replacing the contacts made by tyrosine 340 of the H^+,K^+-ATPase. In contrast, there appeared to be little impairment of function in the M330V, V331I, M334I, or V337I mutants presented here, implying little structural stringency on this surface of M4.

The placement of methionine 334 and valine 337 toward the membrane vestibule conflicts with the currently proposed orientation of M4. A conserved glutamate on the opposite side of the M4 helix from methionine 334 (glutamate 309 in the sr Ca^{2+}-ATPase and 343 in the H^+,K^+-ATPase) is believed to participate in ion binding, making its orientation towards the vestibule an attractive possibility. There is good evidence that this glutamate, found in the conserved sequence V-E-G, is an ion-binding residue. Accordingly, substitution of glutamate 327 in sheep Na^+,K^+-ATPase (*33*) or glutamate 343 in the H^+,K^+-ATPase (*34*) either eliminated or severely lowered apparent affinity for potassium. Loss of Ca^{2+} binding upon substitution of glutamate 309 in sr Ca^{2+}-ATPase has led to its postulated role as a ligand in "site II" for Ca^{2+} (*35*). Finally, the aligned position in the transition-metal P1-type ATPases has a conserved cysteine, a common transition metal ligand. It is possible that both ion and inhibitor gain access to the membrane domain via the vestibule, with the ion eventually moving laterally into a binding site between helices to promote the observed conformational transitions. Ion binding would alter the geometry of the vestibule to exclude inhibitor binding, while inhibitor binding would

distort the ion binding site or prevent ion access to the site. Side-by-side binding of Ca^{2+} in sites designated I and II has been proposed for sr Ca^{2+}-ATPase (*35*) and seems consistent with this type of mechanism.

Alternatively, the ion binding residues may face the vestibule directly, in which case the inhibitor would have to bind between helices. This seems less likely given the size of the inhibitor and apparent lack of required space between helices in the current density maps. It might also be argued that small changes in side-chain volume or orientation represented in M334I and V337I give rise to conformational changes in adjacent side chains that distort the inhibitor site at a distance or even on the opposite side of the helix. The absence of dramatic changes in the kinetic parameters relative to wild type in M334I and V337I, the absence of effects on apparent inhibitor affinity with other mutations in the immediate vicinity of M4, the evidence for protein interaction on the opposing sides of M4, and the fact that at least part of the M4 surface faces the vestibule all seem to weigh against this interpretation.

The effects of side-chain substitution in M334I and V337I allow some conclusions to be made regarding the apparent geometry of the inhibitor binding site. In the case of V337I the addition of a single methyl group lowers the affinity. The bound inhibitor is apparently held rather rigidly adjacent to the valine 337 side chain and there is little flexibility in the site to allow for the volume of an extra methyl group. The linear side chain of methionine, on the other hand, is rather flexible and can adopt a variety of folded conformations that extend several angstroms from the helix backbone. In contrast, the β-branched side chain of isoleucine is restricted to a volume closer to the helix backbone. Exchanging these side chains leads to a 9-fold loss in apparent affinity. Hence a model of the binding site would show the bound inhibitor interacting with the methionine 334 side chain at a distance exceeding the reach of the isoleucine side chain, which cannot provide equivalent contact.

Other recent results are relevant to the structure of the inhibitor site and shed light on the arrangement and orientation of various residues possibly lining the membrane vestibule in the gastric H^+,K^+-ATPase. Antagonism by SCH28080 of omeprazole inhibition of acid transport (*36*) suggested the possibility that the two binding sites overlap. Omeprazole, as a cationic sulfenamide similar in size to SCH28080, inhibits the H^+,K^+-ATPase by disulfide linkage to cysteine 813 (*37*). Recently, a 6-fold increase in the apparent K_i for SCH28080 has been described in a C813T mutant of the H^+,K^+-ATPase prepared and analyzed by the methods described in this report [Lambrecht, N., et al. (2000) *J. Biol. Chem.* (in press)]. In contrast, a C822G mutant showed a $K_{m,app}$ (105 ± 15 nM) equivalent to that of wild type (108 ± 12 nM). These results suggest proximity of cysteine 813, methionine 334, and valine 337. Cysteine 813 is in the sequence P-L-P-L-G-C between M5 and M6, which appears to terminate the M5 helix and form part of the loop before M6. Several other residues whose mutation lowers the apparent affinity for SCH28080 have been identified in M6 by expression of the H^+,K^+-ATPase in HEK293 cells (*31*, *38*). The reported $K_{m,app}$ (K^+) for each mutant can be used to obtain the fraction of V_{max} expected in the presence of 15 mM KCl, the concentration at which inhibition by SCH28080 was tested in these experiments. Half this fractional V_{max} (substituted for the velocity), the IC_{50} found for SCH28080 (substituted for the inhibitor concentration), and the ligand concentration (15 mM K^+) can then be used to solve the equation for a simple linear competitive inhibitor, $V_{max}/v = (K_{m,app}/[S])(1 + [I]/K_{i,app}) + 1$, to obtain the $K_{i,app}$ for each mutant. The calculated $K_{i,app}$ values for SCH28080 in the reported M6 mutants (*31*, *38*) are wild type (42 nM), E820D (313 nM), E820A (156 nM), I816A (369 nM), C822A (95 nM), T823A (425 nM), and P827A (313 nM). The values for wild type and the C822A mutant are in general agreement with those reported here and by N. Lambrecht et al. [*J. Biol. Chem.* (in press)] for C822G. The implied proximity of bound SCH28080 to isoleucine 816, threonine 823, and proline 827 is consistent with the placement of the M5 and M6 segments next to the vestibule as recently proposed (S. Toyoshima, personal communication). Because of the conflicting $K_{i,app}$ for mutants E820D and E820A, where the more radical change in side chain gives less effect on apparent affinity, it remains unclear if glutamate 820 is involved in binding.

ACKNOWLEDGMENT

Primary antibodies mAb HK 12.18 and 2B6 against the H^+,K^+-ATPase α and β subunits were generous gifts from Dr. A. Smolka and Dr. T. Masuda, respectively.

REFERENCES

1. Sachs, G., Chang, H. H., Rabon, E., Schackman, R., Lewin, M., and Saccomani, G. (1976) *J. Biol. Chem. 251*, 7690−8.
2. Besancon, M., Shin, J. M., Mercier, F., Munson, K., Miller, M., Hersey, S., and Sachs, G. (1993) *Biochemistry 32*, 2345−55.
3. Keeling, D. J., Taylor, A. G., and Schudt, C. (1989) *J. Biol. Chem. 264*, 5545−51.
4. Wallmark, B., Briving, C., Fryklund, J., Munson, K., Jackson, R., Mendlein, J., Rabon, E., and Sachs, G. (1987) *J. Biol. Chem. 262*, 2077−2084.
5. Mendlein, J., and Sachs, G. (1990) *J. Biol. Chem. 265*, 5030−6.
6. Im, W. B., Blakeman, D. P., Mendlein, J., and Sachs, G. (1984) *Biochim. Biophys. Acta 770*, 65−72.
7. Kaminski, J. J., Wallmark, B., Briving, C., and Andersson, B. M. (1991) *J. Med. Chem. 34*, 533−41.
8. Kyte, J. (1981) *Nature 292*, 201−4.
9. Lutsenko, S., and Kaplan, J. H. (1995) *Biochemistry 34*, 15607−13.
10. Walderhaug, M. O., Post, R. L., Saccomani, G., Leonard, R. T., and Briskin, D. P. (1985) *J. Biol. Chem. 260*, 3852−9.
11. Smith, D. L., Tao, T., and Maguire, M. E. (1993) *J. Biol. Chem. 268*, 22469−79.
12. Bamberg, K., and Sachs, G. (1994) *J. Biol. Chem. 269*, 16909−19.
13. Corbalan-Garcia, S., Teruel, J. A., Villalain, J., and Gomez-Fernandez, J. C. (1994) *Biochemistry 33*, 8247−54.
14. Zhang, P., Toyoshima, C., Yonekura, K., Green, N. M., and Stokes, D. L. (1998) *Nature 392*, 835−9.
15. Auer, M., Scarborough, G. A., and Kuhlbrandt, W. (1998) *Nature 392*, 840−3.
16. Stokes, D. L., Auer, M., Zhang, P., and Kuhlbrandt, W. (1999) *Curr. Biol. 9*, 672−679.
17. Green, N. M. (1989) *Biochem. Soc. Trans. 17*, 972.
18. Green, N. M., and MacLennan, D. H. (1989) *Biochem. Soc. Trans. 17*, 819−22.
19. Hasler, U., Wang, X., Crambert, G., Beguin, P., Jaisser, F., Horisberger, J. D., and Geering, K. (1998) *J. Biol. Chem. 273*, 30826−35.

20. Bamberg, K., Mercier, F., Reuben, M. A., Kobayashi, Y., Munson, K. B., and Sachs, G. (1992) *Biochim. Biophys. Acta 1131*, 69−77.
21. Reuben, M. A., Lasater, L. S., and Sachs, G. (1990) *Proc. Natl. Acad. Sci. U.S.A. 87*, 6767−71.
22. Chen, B., and Przybyla, A. E. (1994) *BioTechniques 17*, 657−9.
23. Lowry, O. H., Rosenbrough, N. J., Farr, A. L., and Randall, R. J. (1951) *J. Biol. Chem. 193*, 265−275.
24. Laemmli, U. K. (1970) *Nature 227*, 680−5.
25. Rabon, E. C., Im, W. B., and Sachs, G. (1988) *Methods Enzymol. 157*, 649−54.
26. Yoda, A., and Hokin, L. E. (1970) *Biochem. Biophys. Res. Commun. 40*, 880−6.
27. Lorentzon, P., Sachs, G., and Wallmark, B. (1988) *J. Biol. Chem. 263*, 10705−10.
28. Grishin, A. V., and Caplan, M. J. (1998) *J. Biol. Chem. 273*, 27772−8.
29. Clarke, D. M., Loo, T. W., Rice, W. J., Andersen, J. P., Vilsen, B., and MacLennan, D. H. (1993) *J. Biol. Chem. 268*, 18359−64.
30. Munson, K. B., Gutierrez, C., Balaji, V. N., Ramnarayan, K., and Sachs, G. (1991) *J. Biol. Chem. 266*, 18976−88.
31. Asano, S., Matsuda, S., Hoshina, S., Sakamoto, S., and Takeguchi, N. (1999) *J. Biol. Chem. 274*, 6848−54.
32. Green, N. M. (1994) in *The Sodium Pump* (Bamberg, E. S. and Schoner, W., Eds.) pp 110−119, Springer, New York.
33. Kuntzweiler, T. A., Wallick, E. T., Johnson, C. L., and Lingrel, J. B. (1995) *J. Biol. Chem. 270*, 2993−3000.
34. Asano, S., Tega, Y., Konishi, K., Fujioka, M., and Takeguchi, N. (1996) *J. Biol. Chem. 171*, 2740−2745.
35. Rice, W. J., Green, N. M., and MacLennan, D. H. (1997) *J. Biol. Chem. 272*, 31412−9.
36. Hersey, S. J., Steiner, L., Mendlein, J., Rabon, E., and Sachs, G. (1988) *Biochim. Biophys. Acta 956*, 49−57.
37. Besancon, M., Simon, A., Sachs, G., and Shin, J. M. (1997) *J. Biol. Chem. 272*, 22438−46.
38. Asano, S., Matsuda, S., Tega, Y., Shimizu, K., Sakamoto, S., and Takeguchi, N. (1997) *J. Biol. Chem. 272*, 17668−74.
39. Maeda, M., Ishizaki, J., and Futai, M. (1988) *Biochem. Biophys. Res. Commun. 157*, 203−9.
40. Shull, G. E., Schwartz, A., and Lingrel, J. B. (1985) *Nature 316*, 691−5.
41. Crowson, M. S., and Shull, G. E. (1992) *J. Biol. Chem. 267*, 13740−8.
42. Lebovitz, R. M., Takeyasu, K., and Fambrough, D. M. (1989) *EMBO J. 8*, 193−202.
43. Mathews, P. M., Claeys, D., Jaisser, F., Geering, K., Horisberger, J. D., Kraehenbuhl, J. P., and Rossier, B. C. (1995) *Am. J. Physiol. 268*, C1207−14.
44. Gunteski-Hamblin, A. M., Greeb, J., and Shull, G. E. (1988) *J. Biol. Chem. 263*, 15032−40.

BI991837D